Received: 15 October 2023 | Revised: 26 February 2024 | Accepted: 7 March 2024

DOI: 10.1111/jace.19818

Journal of the American Ceramic Society

RESEARCH ARTICLE

Surface ionic coordination of Al_2O_3–CaO–based molten slag induced by structural relaxation

Masanori Suzuki[1] | **Yusuke Asano**[1] | **Yoshiki Ishii**[2]

[1]Graduate School of Engineering, Department of Data Science, Osaka University, Suita, Japan

[2]School of Frontier Engineering, Department of Data Science, Kitasato University, Sagamihara, Japan

Correspondence
Masanori Suzuki, Graduate School of Engineering, Department of Data Science, Osaka University, 2-1 Yamadaoka, Suita, Osaka 565-0871, Japan.
Email: suzuki@mat.eng.osaka-u.ac.jp

Editor's Choice
The Editor-in-Chief recommends this outstanding article.

Funding information
Japan Society for the Promotion of Science, Grant/Award Number: 21H01683

Abstract

The surface tensions of molten oxides depend strongly on the structural relaxation of the surface region. The mechanism of surface structural relaxation for molten oxide slags is complex. The surface tension of calcium aluminate slag is minimal at an intermediate composition, although the critical reason has not been identified. Here, two novel approaches were used to evaluate the features of surface ionic structures in the molten state for the range of 25–50 mol% Al_2O_3: (1) X-ray absorption analysis of oxygen and cationic elements in glass samples after surface relaxation treatment, and (2) molecular dynamics simulations, based on a polarizable-ion model, of the ionic distribution in a molten slag with vacuum/melt interfaces. The results indicate that bridging oxygen (BO) ions are preferred to non-BOs in the surface region. In calcium aluminate slag, BOs are formed by connecting two AlO_4 tetrahedrons with charge compensation of two Al^{3+} ions with one Ca^{2+} ion. Additionally, the above approaches were used to qualify the effect on the surface ionic structure of adding 1–20 mol% SiO_2 to the calcium aluminate slag. The results indicated that the SiO_4 tetrahedrons incorporate the vertex connection with AlO_4 tetrahedrons to form BOs in the surface region.

KEYWORDS
molecular dynamics, slags, surface modification, X-ray methods

1 | INTRODUCTION

The surface tension of molten slag is an important physical property that controls surface phenomena in metallurgical processes, the glass industry, and waste-melting processes. For example, the Marangoni flow of slag, which is driven by local changes in the surface tension is the main cause of local dissolution loss of refractory materials.[1,2] Slag-forming behavior in refining processes[3] and the shapes of weld beads[4] are strongly affected by the surface tension of the molten slag. Control of these phenomena is important because they significantly affect the produced amounts and qualities of materials, and the maintenance costs of refractory materials. Control of these phenomena then requires an understanding and modeling of the surface properties, particularly their composition dependencies. There have been several literatures that evaluated the surface properties and other

physical properties of molten slag and discussed their relations to slag structure.[5–8]

The surface tension of a liquid is often related to the surface free energy per unit area, which is understood as excess energy generated by incomplete bonding of surface atoms.[9] It generally follows that the surface tension increases with increasing strength of the bonds between atoms. However, this simple rule cannot be applied to the surface tensions of molten oxides. For example, although ionic bonding energies are higher than those of metallic bonds, the surface tensions of molten unary oxides are often much lower than those of molten pure metals. Use of the relationship between the surface tension of a molten pure oxide at its melting point and the cationic potential ($U = Z/r$; Z: chemical valence of cation, r: ionic radius of cation) as a measure of the ionic bonding strength[10] does not show a simple trend; MnO, which has a medium cationic potential, has the highest surface tension among molten pure oxides, whereas SiO_2, which has a high cationic potential, has low surface tension.

The effect of surface structural relaxation must be taken into account to explain these complicated trends in the surface tensions of molten oxides.[9,11–12] In unary oxides, it is considered that oxygen ions occupy the surface region because they are larger than the cations and that the electronic state or coordination state between oxygen and the cations can be modified at the surface to decrease the excess surface energy.[13]

For binary or multicomponent oxide systems, surface structural relaxation is much more complicated. For ionic liquids such as molten salts, Tanaka et al. modified the Butler equation to predict the composition dependence of the surface tension by considering the change in the ionic distance at the surface to be a specific aspect of surface relaxation.[11,12] Tanaka and Nakamoto et al. derived a simple semi-empirical model for predicting the surface tension of a molten alkali-metal halide solution by taking account of the ionic radius ratio of the cations and anions, and successfully applied it to silicate systems.[14–16] However, for some oxide systems, the composition dependence of the surface tension is still unpredictable.

We focused on the Al_2O_3–CaO system, which is the fundamental slag system in the secondary refining process in steelmaking, as a typical example of the non-monotonous composition dependence of surface tension. The measured and estimated values of surface tension of the calcium aluminate slag together with those for pure Al_2O_3 and CaO melts are shown in Figure 1. The surface tension of pure Al_2O_3 and CaO melts is measured or estimated as between 600–700 mN / m at their melting points.[21–22] Taking account of its negative temperature dependence, it is interpreted that the surface tension of the Al_2O_3–CaO mixture[17–20] is lower than those of pure Al_2O_3 and CaO

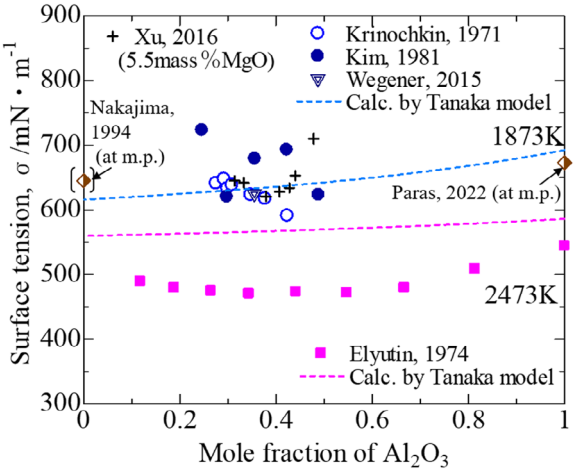

FIGURE 1 The measured and estimated surface tension of Al_2O_3-CaO melt.

melts (estimated as 700–800 mN/m at 1873 K, and therefore shows a minimum at an intermediate composition.[19] Additionally, it has been reported that the surface tension of the Al_2O_3-CaO-MgO melts with fixed MgO mass content shows the minimum at an intermediate composition against the Al_2O_3/CaO mass ratio.[23] In contrast, the calculated results[15] show a monotonous composition dependence and therefore cannot reproduce the minimum. The special trend in the measured surface tension can be attributed to surface structural relaxation. However, the mechanism of surface structure modification, and the difference between the ionic structure at the surface and in the bulk region, have not been clarified. The effect of the CaO / Al_2O_3 ratio on the surface properties of molten CaO-Al_2O_3-based slag has been investigated in several previous studies,[5,6] but the structural features in the surface region are still not fully understood.

In addition, the effect of SiO_2 addition as a minor component on the surface ionic structure has not been clarified. Although it is known that SiO_2 acts as a surface active component in a molten slag and significantly decreases the surface tension,[24] it is unclear how the ionic structure is modified in the surface region by the addition of a small amount of SiO_2; surface segregation is a possible mechanism.

The purpose of this study was to clarify the features of the surface ionic structures of Al_2O_3–CaO and Al_2O_3–CaO–SiO_2 slags that could be the key factors that explain the composition dependence of surface tension. Two novel approaches were used to examine the surface ionic structure of the slag: (i) X-ray absorption spectroscopy investigation of oxygen and the cationic elements by using electron and fluorescence yields, and (ii) molecular dynamics (MD) simulations of systems including vacuum/liquid interfaces.

2 | EXPERIMENTAL PROCEDURE

In this study, X-ray absorption spectroscopy was used to examine the local coordination states of oxygen and cationic elements at the surface region of an oxide glass after surface ionic structural relaxation. X-ray absorption near edge structure (XANES) spectroscopy is used to determine the chemical valence and coordination state of a target element.[25] Soft X-ray absorption spectroscopy provides different methods for recording XANES spectra. The electron yield detects the amount of surface electrons as an electrical current and is surface-dependent (up to several to 10 nm in depth from the top surface). The fluorescence yield detects the fluorescence X-ray intensity and is bulk-dependent (deeper than several tens of micrometers from the top surface).[26] The advantage of electron-yield XANES is that the given structural information is more detailed than that obtained with X-ray photoelectron spectroscopy (XPS) because electron-yield XANES reflects both auger and photoelectrons, whereas XPS reflects only photoelectrons.[27] In this study, we used XANES spectroscopy to study an oxide glass instead of a high-temperature melt, under the assumption that the surface ionic structure of the glass after structural relaxation is similar to that of the melt. When annealing the crushed oxide glass sample, the relaxation of the surface ionic structure proceeds to reduce surface excess energy caused by partially incomplete ionic bonding, which is similar to the proposed mechanism of surface relaxation for ionic melt.[11,12] If the glassy state is kept in the surface region, we could consult the surface ionic structure of the annealed glass sample as the first approximation to understand the surface structure relaxation of the oxide melt.

Two composition ranges were selected for glass preparation. Series A contained 30–50 mol% Al_2O_3 in the Al_2O_3–CaO system; this includes the composition that potentially gives the minimum surface tension in the molten state. In series B, 1–20 mol% SiO_2 was added to an Al_2O_3–CaO system with a fixed Al_2O_3/CaO molar ratio of 7/12. Table 1 lists the chemical compositions of the glass samples.

The glass samples were prepared as follows. First, calcium carbonate (special grade, Fujifilm Wako Chemicals Co., Ltd.) was calcined at 1223 K in air overnight to form CaO. Then Al_2O_3 and SiO_2 (both special grade, Fujifilm Wako Chemicals Co., Ltd., Tokyo, Japan) and the CaO were mixed in the powdered state and pressed into a pellet at 10 MPa for 15 min. The pellet was cut into pieces of diameter 1–2 mm and then melted by using laser irradiation. The aerodynamic-levitation and laser-irradiation technique enables the effective melting of oxide samples with high liquidus temperatures, without contamination from the container, and quenching into a glassy state by rapid cooling.[28–30] The sample was aerodynamically levitated by an Ar gas flow (99.999% purity) from a nozzle at the bottom of the chamber and heated by a 100 W CO_2 gas laser (Firestar ti100, Synrad Co. Ltd.; wavelength 1.6 μm, laser diameter 2 mm) up to 2273 K in air. The sample temperature was measured by a pyrometer and the emissivity was calibrated to reproduce the melting point of Al_2O_3. The levitated slag sample was melted at 2073–2273 K, held at 1873–1973 K for 10 min, and then quenched by turning the laser power off. In this case, the cooling rate was higher than −500 K/s. Next, the glass samples were annealed at 873 K for 24 h in air to adjust structural distortion. The glass sample was then crushed into a powder in the air, which induced the formation of a large surface area with incomplete surface relaxation. Surface structural relaxation was promoted by annealing the powder sample at 873 K for 48 h. This annealing temperature was determined to be lower than the glass-transition temperature estimated by using Sakka's relation[31] ($T_g/T_L = 2/3$, where T_g is the glass-transition temperature and T_L is the liquidus temperature) to avoid crystallization.

TABLE 1 Chemical compositions of glass samples used in this study.

Sample name	Composition (mol%)		
	Al_2O_3	CaO	SiO_2
A1	30	70	0
A2	36.8	63.2	0
A3	50	50	0
B1	36.5	62.5	1
B2	35	60	5
B3	33.2	56.8	10
B4	29.5	50.5	20

The soft X-ray absorption measurements were performed at the BL-10 and BL-11 beamlines at the Ritsumeikan University SR Center (Shiga, Japan). The powdered glass samples and SiO_2 glass, and α-Al_2O_3 and Mayenite ($Ca_7Al_{12}O_{33}$) crystals as reference materials, were individually attached to a pure indium plate on the sample holder to support electrical conduction, and these holders were placed in the sealing vessel. These preparations were performed in a glovebox in a dry Ar atmosphere to avoid moisture absorption. The vessel with the samples was attached to the soft X-ray absorption spectroscopy facility and absorption measurements were performed under a high vacuum (less than 10^{-6} Pa). The O K-edge XANES spectrum was obtained at BL-11 in both partial electron yield (PEY) and partial fluorescence yield (PFY) modes using a diffraction grating with 1200 lines/mm. The

Al and Si K-edge XANES spectra were obtained at BL-10 in the total electron yield (TEY) and PFY modes by using $KTiOPO_4$ (011) and InSb (111) dispersive crystals. The latest version of the Athena program[32] was used to draw the background lines using a spline function and to normalize the recorded spectra.

3 | COMPUTATIONAL METHODOLOGY

In this study, classical MD calculations based on a polarizable-ion model (PIM-MD) were performed to simulate the ionic distributions in Al_2O_3–CaO and Al_2O_3–CaO–SiO_2 melts with included vacuum/liquid interfaces. The PIM evaluates the dipole moment between each ion, $\boldsymbol{\mu_i}$, from the multiple of the polarization parameter, α_i, and the electric field, $\boldsymbol{E_i}$, generated at the position of the focused ion by the whole set of charges and induced dipoles ($\boldsymbol{\mu}_i = \alpha_i \cdot \boldsymbol{E}_i$).[33–37] The potential energy function is decomposed into four parts, and expressed as:

$$\phi_{\text{Total}} = \phi_{\text{Charge}} + \phi_{\text{Dispersion}} + \phi_{\text{Repulsion}} + \phi_{\text{Polarization}} \tag{1}$$

The charge term corresponds to the coulombic interaction between two ions i and j, that is,

$$\phi_{\text{Charge}} = \frac{q_i q_j}{r_{ij}} \tag{2}$$

where q_i is the charge on each ion i and r_{ij} represents the distance between the two ions. The dispersion term, $\phi_{\text{Dispersion}}$, which corresponds to the instantaneous correlations of density fluctuations between electron clouds is expressed as

$$\phi_{\text{Dispersion}} = -\sum_{i<j}\left[f_6^{ij}\frac{C_6^{ij}}{(r_{ij})^6} + f_8^{ij}\frac{C_8^{ij}}{(r_{ij})^8}\right] \tag{3}$$

where C_6^{ij} and C_8^{ij} represent the dipole–dipole and dipole–quadrupole dispersion coefficients.

The term f_n^{ij} represents the damping functions that correct the short-range interactions:

$$f_n^{ij} = 1 - c_n^{ij} e^{-b_n^{ij} r_{ij}} \sum_{k=0}^{n} \frac{\left(b_n^{ij} r_{ij}\right)^k}{k!} \tag{4}$$

where the inverse of b_n^{ij} corresponds to the damping range. The repulsion term, $\phi_{\text{Repulsion}}$, is expressed by the decay functions as

$$\phi_{\text{Repulsion}} = \sum_{i<j} A_{ij} e^{-B_{ij} r_{ij}} \tag{5}$$

where A_{ij} and B_{ij} are parameters determined between two types of ions i and j. The polarization term, $\phi_{\text{Polarization}}$, consists of charge–dipole and dipole–dipole interactions, and the energy cost for deforming the electric fields of ions:

$$\phi_{\text{Polarization}} = \sum_{i<j}\left[\frac{q_i \boldsymbol{r_{ij}}\cdot\boldsymbol{\mu_j}}{r_{ij}^3} f_4^{ij} - \frac{\boldsymbol{\mu_i}\cdot q_j \boldsymbol{r_{ij}}}{r_{ij}^3} f_4^{ij} + \frac{\boldsymbol{\mu_i}\cdot\boldsymbol{\mu_j}}{r_{ij}^3} - \frac{3\left(\boldsymbol{r_{ij}}\cdot\boldsymbol{\mu_i}\right)\cdot\left(\boldsymbol{r_{ij}}\cdot\boldsymbol{\mu_j}\right)}{r_{ij}^5}\right] + \frac{|\mu_i|^2}{2\alpha_i} \tag{6}$$

In practice, the instantaneous dipole moments are determined at each time step by minimization of the total energy by using the conjugate gradient method.

The parameters for the PIM force field in Equations (1)–(6) are listed in Tables S1 and S2; they were determined to reproduce the force and dipole moment calculated by using first-principles MD calculations for identical oxide systems in the glassy and molten states.

The calculations were performed as follows to simulate the distributions of ions induced by surface relaxation in oxide melts. First, a cubic cell containing around 3000 atoms was held at 2273 K for 30 ps and equilibrated at 2073 K for 30 ps, by using a rigid-ion model (RIM) that neglected the polarization term for the potential energy in Equation (1), and then for 100 ps by using PIM to achieve a steady value of the cell total energy. Next, the equilibrated ionic configuration was extended 3–6 times in a uniaxial direction and then equilibrated again at 2073 K in the same way as above. Vacuum spaces were inserted in the upper and lower sides of the rectangular cell to introduce vacuum/liquid interfaces, and the cell was equilibrated using a RIM and PIM. All these calculations were performed in the *NVT* ensemble, where N is the number of particles, V is the volume, and T is the temperature. In the realistic phenomena, gas molecules existing in the vapor phase may also involve surface properties in the oxide melts.[7] However, when comparing the number of molecules included in melting and vapor phases, the relative number of gas molecules is small and almost zero in the present simulation size. In addition, representative gas molecules do not have molecular charges, and they are light as weight. Therefore, in the present MD simulation, the effect of gas molecules on the surface structure of the oxide melt was recognized as trivial.

The ionic coordination between oxygen and cations in the equilibrated cell was analyzed by using the tetrahedral order parameter q,[37,38] which describes the polymorphic distribution based on the tetrahedral state, by using the

bond angles:

$$q = 1 - \frac{3}{8}\sum_{j=1}^{n-1}\sum_{k=j+1}^{n}\left(\cos\theta_{ijk} + \frac{1}{3}\right)^2 \quad (7)$$

where θ_{ijk} represents the angle formed between the central Si or Al atom, denoted by j, and its neighboring oxygen atoms, denoted by i and k. The distribution of the bond angle M–O–N (M and N are either a Si or Al atom) was analyzed to examine the connecting states between the polymorphs. The equilibrated rectangular cell was divided into several layers of thickness approximately 20 Å, and the distributions of Si- or Al-centered polymorphs and the M–O–N bond angles were separately analyzed for the upper and lower (corresponding to the surface region), and middle (corresponding to the bulk region) layers.

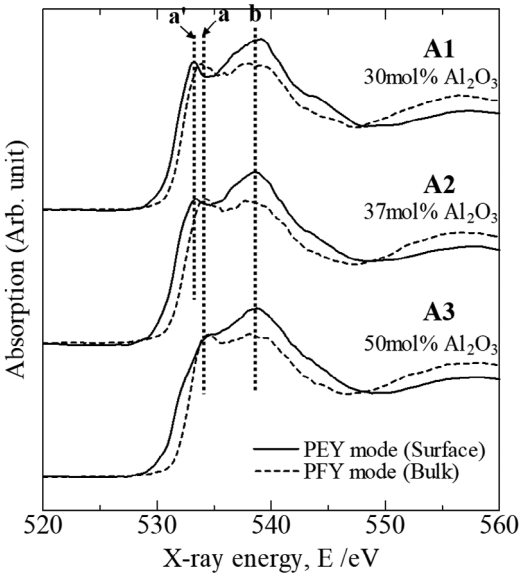

FIGURE 2 O K-edge X-ray absorption near edge structure (XANES) spectra of the Al_2O_3-CaO glasses A1-A3 after surface relaxation.

4 | RESULTS AND DISCUSSION

4.1 | XANES spectroscopic examination of glass after surface relaxation

A. Al_2O_3–CaO system

First, the observed O K-edge XANES spectra of the A2 glass powder before and after the annealing are shown in Figure S1 in supplementary materials, to verify the effect of the annealing for the surface relaxation of the glass on the ionic structure. The PFY spectra did not change during the annealing, indicating that bulk structural distortion was already removed before the crushing. In contrast, the PEY spectra reflecting surface structure clearly changed by the annealing, where the intensity of the absorption peak a' increased relatively to peak b. This result indicated that the annealing contributed to the surface structure relaxation of the glass powder.

Figure 2 shows the O K-edge XANES spectra of Al_2O_3–CaO glasses of different compositions after surface relaxation. All the spectra show two broad absorption peaks (a or a', and b). Peaks a and a' correspond to Al–O–Ca non-bridging oxygen (Al-NBO) and peak b represents Al–O–Al bridging oxygen (Al-BO).[39] Regardless of the glass composition, the intensity of the Al-BO peak (b) in the surface spectrum was higher than that of the Al-NBO peak (a'). This trend became more significant with increasing Al_2O_3 content in the range of 30–50 mol% Al_2O_3. In contrast, in the bulk spectra, the intensities of the two peaks were comparable, and its compositional dependence was not significant. It should be noted that the PFY spectra may have been flattened because of the self-absorption effect, but the ratio of the two peak intensities should be unchanged. Jiang et al.[40] reported that the pre-edge peak at 528 eV was observed in the O K-edge electron energy-loss spectroscopy of some oxide minerals containing alkaline elements by using the high voltage electron microscopy, which was attributed to the formation of free O_2 gas by radiation damage. Then, Henderson et al.[39] previously discussed the effect of radiation damage on the intensity ratio of the TEY spectra of the calcium aluminate mineral. Because in the case of electron microscopy, the high energy electron beam is irradiated to the localized area of the sample, such radiation damage would occur. However, the surface spectra in this study did not show the pre-edge peak corresponding to the radiation damage. The soft X-ray is irradiated broadly to the sample, and in the PEY spectrum, the effect of the radiation damage would have been small because the electron spectrum with higher energies than blocking voltage was extracted. Consequently, these spectra results indicate that Al-BO is preferentially distributed in the surface rather than in the bulk of the glass. In addition, for glasses A1 and A2, the peak energies for Al–NBO coordination in the surface spectra were negatively shifted relative to those in the bulk spectra. As previously reported,[41] such deviations in the peak positions may result from differences between the Ca-fold structures in each region.

Figure 3 shows the Al K-edge XANES spectra of the Al_2O_3–CaO glasses after surface relaxation. All the spectra show two absorption peaks (c and d), which correspond to Al^{3+} cations that are tetrahedrally (c: 1565 eV by Kato et al.[42]) or octahedrally coordinated (d: 1568 eV by Kato, McKeown and Cabaret[42–44]) with oxygen anions. In the bulk spectra, while Al_2O_3 content increased, the ratio of

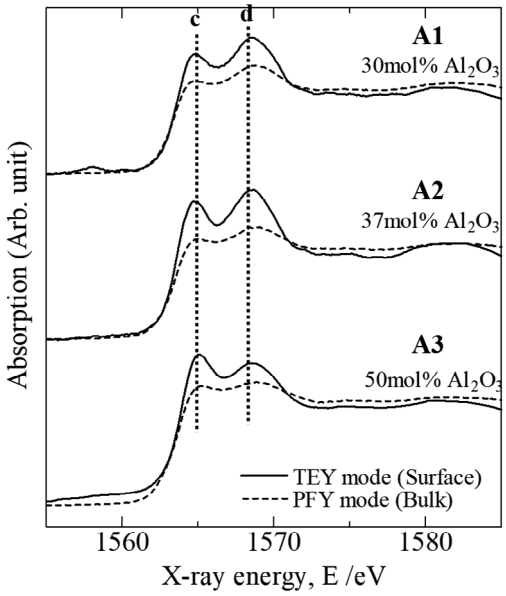

FIGURE 3 Al K-edge X-ray absorption near edge structure (XANES) spectra of the Al_2O_3-CaO glasses A1-A3 after surface relaxation.

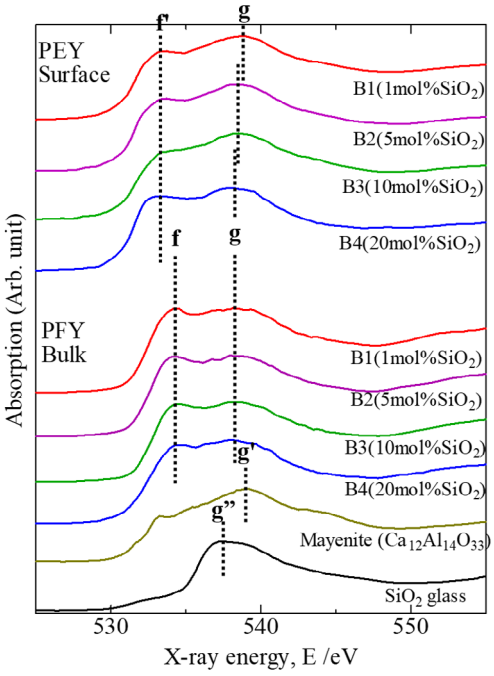

FIGURE 4 O K-edge X-ray absorption near edge structure (XANES) spectra of the Al_2O_3-CaO-SiO2 glasses B1-B4 after surface relaxation.

the c and d peak intensities did not change much. However, in the surface spectra, the intensity of the c peak increased significantly compared with that of the d peak. This trend indicates that AlO_4 coordination is preferred in the surface region, particularly with increasing Al_2O_3 content, where Al-BO could be formed by the connection of two AlO_4 tetrahedrons.

These results suggest that in the surface regions of the Al_2O_3–CaO glasses, the formation of the Al-BO structure occurs preferentially after surface relaxation. It should be noted that one Ca^{2+} cation must be supplied for charge compensation to form two AlO_4 tetrahedrons.[45–47] Thus, this structure can be formed only at intermediate compositions of the Al_2O_3–CaO system.

B. Al_2O_3–CaO–SiO_2 system

Figure 4 shows the O K-edge XANES spectra of the Al_2O_3–CaO–SiO_2 glasses after heat treatment for surface relaxation. In contrast to the case for the bulk spectra, in the surface spectra, the intensity of the BO absorption peak (g) was higher than that of the NBO peak (f). In addition, the peak energy for NBO coordination (f') in the surface spectra was lower than that in the bulk spectra (f). With increasing SiO_2 content, the BO peak energy in the surface spectra became slightly lower, and approached that of the absorption peak corresponding to Si–O–Si BO (g") in the spectrum of silica glass. However, in the bulk spectra, a shift in the BO peak energy was not clearly observed.

Figure 5 shows the Al K-edge XANES spectra of the Al_2O_3–CaO–SiO_2 glasses after surface relaxation. The spectra show two absorption peaks corresponding to AlO_4 (c) and AlO_6 (d) coordination states. With increasing SiO_2 content, the intensities of the AlO_4 peaks in the surface spectra increased significantly and exceeded those of the AlO_6 peaks. In the bulk spectra, the intensity ratio of these two peaks did not change much. This may indicate that in the surface region, selective distribution of the AlO_4 coordination state can be achieved by increasing the SiO_2 content.

Figure 6 shows the Si K-edge XANES spectra of the Al_2O_3–CaO–SiO_2 glasses after surface relaxation. When the SiO_2 content was 1 mol%, the spectra of both the surface and bulk regions showed a broad absorption peak. The main Si-coordination state therefore could not be clearly determined. However, with increasing SiO_2 content, both spectra showed the specific features of individual coordination states. The bulk spectra clearly showed two absorption peaks (h and i). The peak energy h corresponds to that observed for grossular ($Ca_3Al_2[SiO_4]_3$),[48] in which a Si cation is tetrahedrally coordinated with neighboring oxygen anions, and the SiO_4 tetrahedron is surrounded by an AlO_6 octahedron through NBO ions in the crystal structure (Si^{IV}–O–Al^{VI}). The other peak, i, corresponds to an octahedrally coordinated Si cation (SiO_6), which has been found in the silicon phosphate SiP_2O_7.[49] When SiO_2 is a minor component in the glass, Si cations, therefore, show both tetrahedral and octahedral coordination states in the bulk region. In contrast, the surface spectrum shows only one broad absorption peak. When the SiO_2 content was

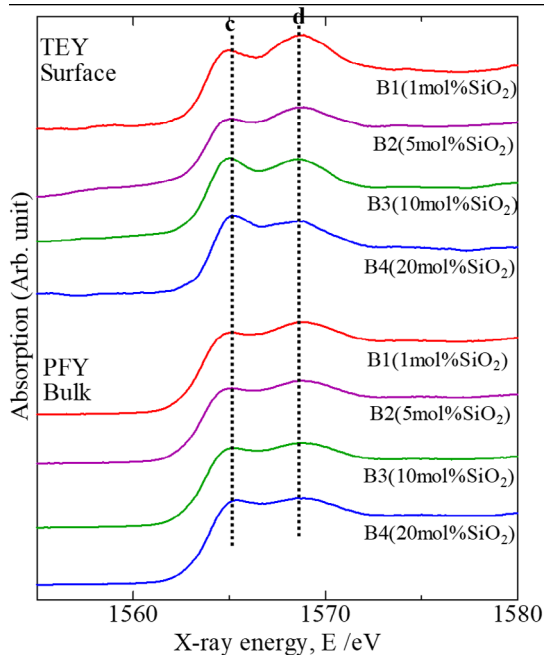

FIGURE 5 Al K-edge X-ray absorption near edge structure (XANES) spectra of the Al_2O_3-CaO-SiO2 glasses B1-B4 after surface relaxation.

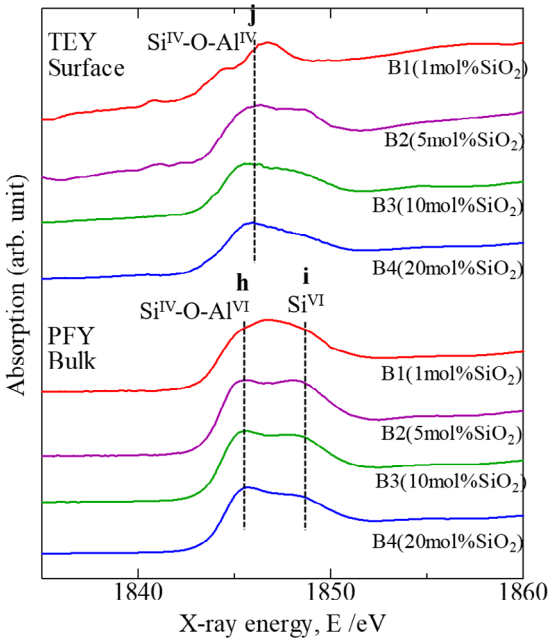

FIGURE 6 Si K-edge X-ray absorption near edge structure (XANES) spectra of the Al_2O_3-CaO-SiO2 glasses B1-B4 after surface relaxation.

increased, the central peak shifted to the one (j) observed for anorthite ($CaAl_2Si_2O_8$),[47] in which a SiO_4 tetrahedron is connected with four AlO_4 (Si^{IV}–O–Al^{IV}) tetrahedrons through BO ions.

These XANES spectroscopic results indicate that the dominant coordination state in the surface region changes from Al^{IV}–O–Al^{IV} to Si^{IV}–O–Al^{IV} when small amounts of SiO_2 are added; both states involve BO.

4.2 | MD simulation of an ionic structure after surface relaxation

A. Al_2O_3–CaO system

Figure 7 shows the ionic distribution in a cell of a $25Al_2O_3$–75CaO (mol%) melt with vacuum/liquid interfaces after structural relaxation. Figure 7 shows the change in the total energy of the melt (potential energy + kinetic energy + polarization energy) per calculation step (1 step = 1 fs). The total energy decreased and achieved a certain value in 90,000 steps under RIM and PIM, respectively. The results indicate that the cell with vacuum/liquid interfaces achieved an equilibrium state.

Figure 8 shows the distribution of AlO_n polymorphs in different layers in the equilibrated cell of a $25Al_2O_3$–75CaO (mol%) melt, based on the q parameter as expressed in Equation (7). Layers 1 and 9 are those directly exposed to the vacuum space (surface), and layer 5 represents the bulk region. Three Al–O coordination states (AlO_4, AlO_5, and AlO_6) were identified. In the surface layer, the proportion of AlO_4 coordination was slightly higher, and those of AlO_5 and AlO_6 were lower than average. The bulk region had a lower proportion of AlO_4 and higher proportions of AlO_5 and AlO_6 than average. This indicates that AlO_4 is the preferred Al–O coordination state in the surface layer.

Figure 8 shows the distributions of Al–O–Al bond angles in different layers. Two broad peaks were identified. Peak θ_1 (~100°) corresponds to the edge connection of two polymorphs through two oxygen anions; the other peak, θ_2 (~125°), represents a vertex connection of two tetrahedrons through one BO ion.[34] The surface region (layers 1 and 9) showed a slightly higher proportion of θ_2 but a lower proportion of θ_1 compared with the average and those in the bulk region (layer 5). This indicates that the vertex connection of two AlO_4 tetrahedrons with one BO (Al^{IV}–O–Al^{IV}) is preferred in the surface region.

Figure 9 shows the ionic structure in the cell of a $50Al_2O_3$–50CaO (mol%) melt with vacuum/liquid interfaces after structural relaxation, and Figure 9 shows the distribution of AlO_n polymorphs in the equilibrated cell. Layers 1 and 7 represent the surface, and layer 4 corresponds to the bulk region. The results clearly show that AlO_4 coordination is preferred in the surface layers, although AlO_5 is dominant on average and in the bulk region.

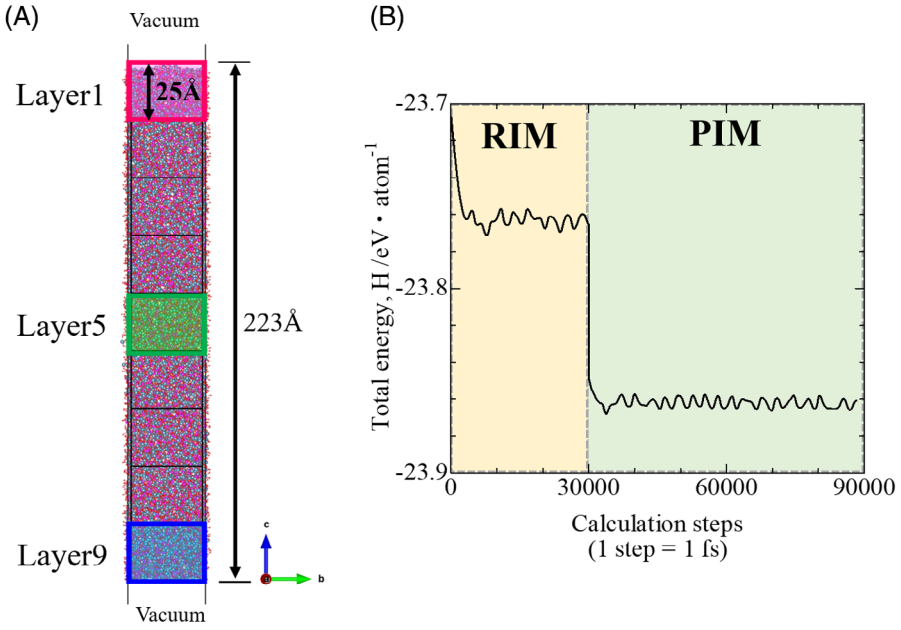

FIGURE 7 (A) Ion distribution in the cell of 25 Al_2O_3-75 mol% CaO melts with vacuum / liquid interfaces after structural relaxation. (B) Change in total energy by calculation step (1 step = 1 fs).

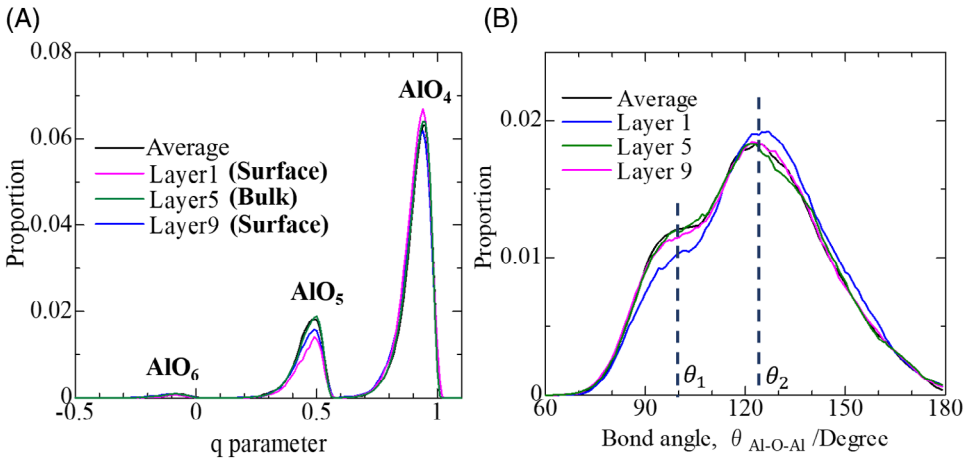

FIGURE 8 Distributions of (A) AlOn polymorphs and (B) Al-O-Al bond angle, in the cell of 25 Al_2O_3-75 mol% CaO melt with vacuum / liquid interfaces after structural relaxation.

Figure 9 shows the distribution of Al–O–Al bond angles in different layers in the equilibrated cell of a $50Al_2O_3$–50CaO (mol%) melt. At the average distribution, the proportion of peak θ_1 (~100°) is highest, and the second peak, θ_2 (~125°), shifted negatively from that in the $25Al_2O_3$–75CaO (mol%) melt. This is attributed to the increased proportions of AlO_5 and AlO_6 polymorphs relative to AlO_4, some of which are connected at the vertex (Al^{IV}–O–Al^{V} or Al^{V}–O–Al^{V}) by lower bond angles than that of the Al^{IV}–O–Al^{IV} connection. However, in the surface region, a vertex connection of polymorphs is preferred, whereas the edge connection is declined.

These results indicate that the surface region of the Al_2O_3–CaO melt shows a preferential distribution of AlO_4 tetrahedrons, which partially contribute to the formation of BO ions via vertex connections.

In terms of Ca-O coordination, the CaO_n polymorphs distributions in the equilibrated cells of these Al_2O_3–CaO melts (Figure S2: (a) 25 Al_2O_3-75 mol% CaO, (b) 50 Al_2O_3-50 mol% CaO) demonstrate that the polymorphs with low coordination numbers (e.g., CaO_4 or CaO_5) are preferred but those with higher coordination numbers are declined in the surface region. They support the interpretation of O K-edge XANES of the Al_2O_3–CaO glasses, featured

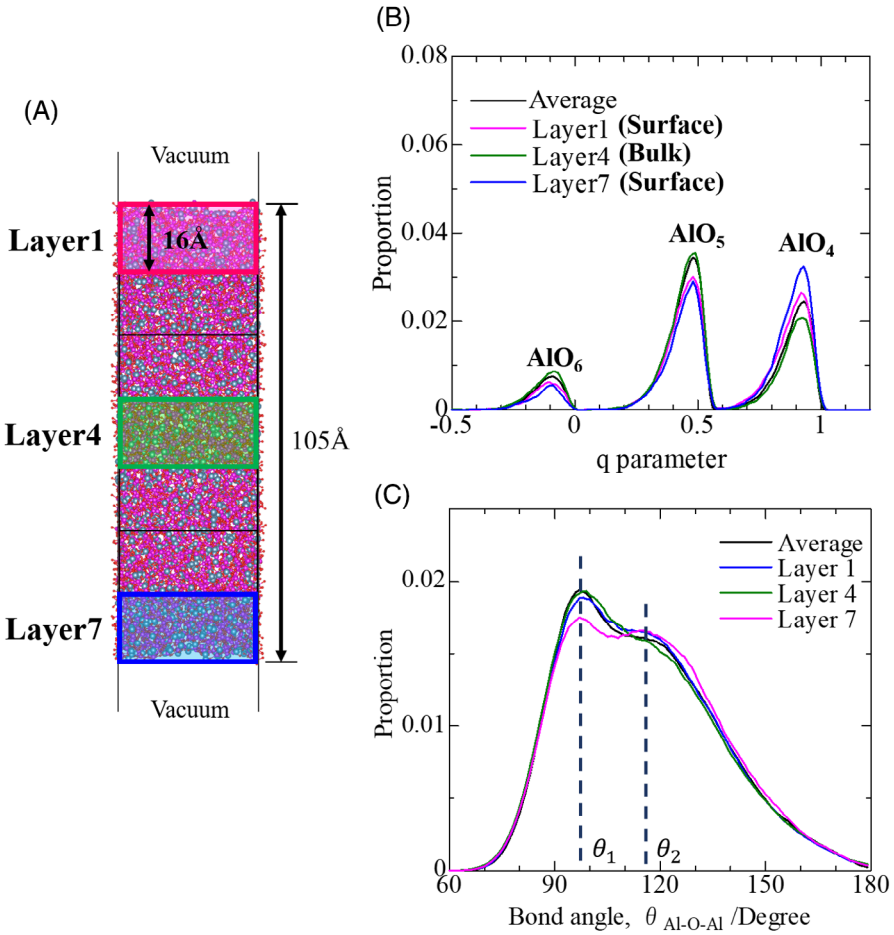

FIGURE 9 (A) Ion distribution, (B) distribution of AlOn polymorphs, and (C) Al-O-Al bond angle, in the cell of 50 Al_2O_3-50 mol% CaO melt with vacuum/liquid interfaces after structural relaxation.

by a negative shift of the Al-NBO peak in the surface spectra.

For comparison with calcium aluminate melts, the surface-relaxed structure in pure Al_2O_3 and CaO melts near these melting points were evaluated by PIM-MD simulation. The results are shown in Figures S3 and S4 in supplementary materials, respectively. The results indicate that the polymorphs of low coordination numbers become slightly preferred in the surface region (e.g. AlO_4 for Al_2O_3 melt and CaO_5 for CaO melt), whereas no change is observed in the cation-oxygen-cation bond angle between surface and bulk region. Therefore, the changes between surface and bulk region in both Al-O coordination and Al-O-Al bond angle are observed only for calcium aluminates.

B. Al_2O_3–CaO–SiO_2 system

The results for a $37Al_2O_3$−63CaO (mol%) melt with 5 and 20 mol% SiO_2 are presented.

The ionic distributions in cells with vacuum/liquid interfaces and 5 and 20 mol% SiO_2 addition after equilibration are represented in Figure S5A,B. Al, Ca, and Si cations were homogeneously dispersed in the liquid, therefore Si segregation was not observed.

Figure 10 shows the distributions of SiO_n polymorphs in different layers for the cases with 5 and 20 mol% SiO_2 addition, respectively. When the SiO_2 content was 5 mol%, various Si–O coordination states including octahedral coordination as dominant were observed. In the surface region, the proportion of SiO_4 tetrahedrons was slightly higher, but those of other polymorphs were lower than those in the bulk region. When the SiO_2 content increased to 20 mol%, SiO_4 tetrahedrons predominated. In this case, there were no specific differences between the SiO_n distributions in the surface and bulk regions.

Figure 11 shows the distributions of AlO_n polymorphs in the surface and bulk regions. The results for the surface region are presented as the average of the distributions in the two layers directly exposed to the vacuum/liquid interfaces. Regardless of the SiO_2 content, AlO_5 was identified as the major Al–O coordination state; AlO_4 and AlO_6 were also identified. When the SiO_2 content was 5 mol%, the AlO_n distributions in the surface and bulk

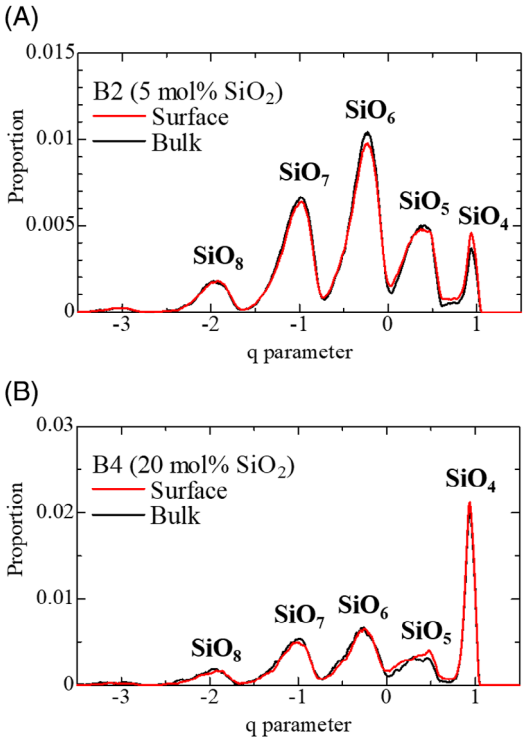

FIGURE 10 Distribution of SiOn polymorphs in the cells of Al_2O_3-CaO-SiO_2 melts with vacuum/liquid interfaces after structural relaxation. (A) B2 (5 mol% SiO_2) and (B) B4 (20 mol% SiO_2).

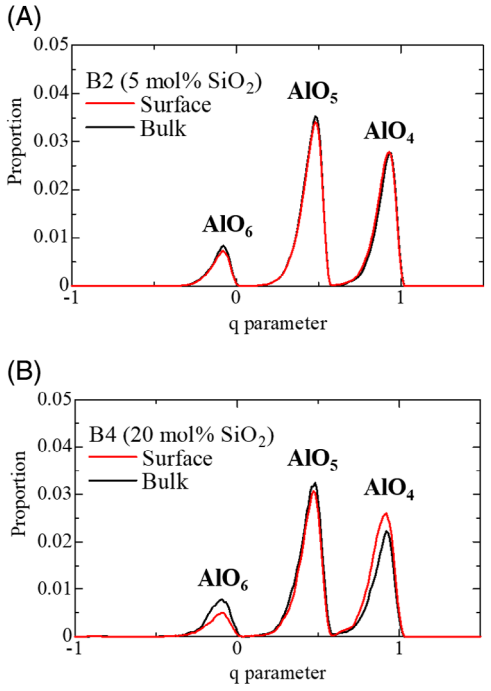

FIGURE 11 Distribution of AlOn polymorphs in the cells of Al_2O_3-CaO-SiO_2 melts with vacuum/liquid interfaces after structural relaxation. (A) B2 (5 mol% SiO_2) and (B) B4 (20 mol% SiO_2).

regions were comparable. However, when the SiO_2 content was 20 mol%, compared with the bulk region, the surface region clearly showed a preferential distribution of AlO_4 tetrahedrons rather than AlO_5 and AlO_6.

The polymorph connectivities were investigated. The distributions of the Si–O–Si, Al–O–Si, and Al–O–Al bond angles are shown in Figures S6–S8, respectively, in supplementary materials. Note that the distribution of the Si–O–Si bond angle for the case of 5 mol% SiO_2 could not be analyzed because most of the SiO_n polymorphs were disconnected from each other. In the case of 20 mol% SiO_2, the Si–O–Si bond angle distributions in both the surface and bulk regions showed a single broad peak at θ_2 (~130°), which corresponds to the vertex connection of two SiO_4 tetrahedrons through one BO ion (Si^{IV}–O–Si^{IV}).[34] The surface region gave a sharper peak than the bulk region did, which indicates that the connection between two SiO_4 tetrahedrons tends to be ordered in the surface region (Figure 11).

The distributions of the Al–O–Si bond angle in the surface and bulk regions differed significantly when the SiO_2 content was 5 mol%. The peak at θ_1 (~100°) corresponds to the edge connection, and that at θ_2 (~125°) corresponds to the vertex connection, of two polymorphs. In particular, the vertex connection of AlO_4 and SiO_4 tetrahedrons (Si^{IV}–O–Al^{IV}) is accompanied by one BO ion. The surface region showed preferential distribution of vertex connections. When the SiO_2 content increased to 20 mol%, θ_1 became the minor peak, and θ_2 predominated. This indicates that the Si^{IV}–O–Al^{IV} vertex connection became the main configuration between AlO_n and SiO_n polymorphs. In this case, there were no specific differences between the surface and bulk regions.

The distribution of the Al–O–Al bond angle for the case of 5 mol% SiO_2 showed two peaks at θ_1 (~100°) and θ_2 (~120°). The distributions in the surface and bulk regions were comparable. When the SiO_2 content increased to 20 mol%, the distribution in the surface region showed a slightly higher proportion at the θ_2 peak but a lower proportion at the θ_1 peak, than those in the bulk region. These results indicate that vertex connection between the AlO_n polymorphs is preferred in the surface region.

The above results clearly indicate that SiO_2 addition significantly affects the distribution of the AlO_n in the melt. Si cations prefer tetrahedral coordination with oxygen ions, and AlO_4 and AlO_5 become minor and major coordination states, respectively. However, in the surface region, the distribution of tetrahedrons (AlO_4 and SiO_4) is preferred, some of which form BO ions via vertex connections, for example, Si^{IV}–O–Si^{IV}, Al^{IV}–O–Si^{IV}, and Al^{IV}–O–Al^{IV}. This trend is consistent with the XANES spectroscopic analysis of the Al_2O_3–CaO–SiO_2 glass structure. In addition, the PIM-MD simulation enabled the identification of the categories of Al- or Si-related polymorphs and

the quantitative evaluation of the proportions of these polymorphs.

5 | SUGGESTED SURFACE IONIC STRUCTURE IN CALCIUM ALUMINOSILICATE MELT

The results of XANES spectroscopic analysis of the glass after surface relaxation and the MD simulation of the melt structure indicate the preferential formation of BO ions in the surface region by the selective distribution of tetrahedrons such as AlO_4 or SiO_4, and their vertex connections. This can be explained as follows. Because they form strong covalent bonds with the nearest cations, the formation of BO ions significantly decreases the excess surface energy, which is related to the surface tension. Therefore, they are preferentially distributed in the surface region by surface relaxation of the melt.

For a calcium aluminate slag, AlO_4 is preferentially formed in the surface region, rather than AlO_5 or AlO_6. These AlO_4 units selectively form vertex connections, with an accompanying BO ion (Al^{IV}–O–Al^{IV}). However, note that AlO_4 tetrahedron formation requires the presence of Ca^{2+} ions for charge compensation. The above mechanism of surface relaxation is therefore likely to occur in Al_2O_3–CaO melts with intermediate compositions. Both the XANES analysis and MD simulations in the range of 25 – 50 mol% Al_2O_3 indicated that the preferential distributions of the AlO_4 tetrahedrons and BOs become more significant as increasing Al_2O_3 content.

The ionic configurations in the surface of the Al_2O_3–CaO–SiO_2 melt are suggested to be as follows. When the SiO_2 content is lower than 5 mol%, the preferential formation of Si^{IV}–O–Al^{IV} vertex connections provides more BO ions in the surface area than in the bulk region. When the SiO_2 content is 20 mol%, additional BO ions are supplied by the preferential formation of Si^{IV}–O–Si^{IV} and Al^{IV}–O–Al^{IV} connections, and Al^{IV}–O–Si^{IV} connections are also present. SiO_2 addition therefore significantly affects the surface ionic structure, which directly changes the surface tension of the calcium aluminate slag. Taking account of the thickness of the actual surface region being even thinner than several nanometers, the difference in the distribution of structural species between surface and bulk would be more significant than observed in this study.

When the fundamental equation by Butler.[50] to predict surface tension of a mixture is taken into account, the surface tension of the oxide melt could be changed proportionally by the logarithm of the population ratio of the structural species (e.g., Si^{IV}–O–Si^{IV} or Al^{IV}–O–Al^{IV}) in the surface and bulk regions, as well as by the differences of partial interaction energies of these structural species, relating to their connecting states, between surface and bulk regions. The partial interaction energies of the structural species in the surface region of the oxide melt have not been understood yet. Therefore, the modeling of structural relaxation on the surface tension of oxide mixture slag is required for our future study.

6 | CONCLUSION

In this study, for the first time, the structural features in the surface areas of Al_2O_3–CaO and Al_2O_3–CaO–SiO_2 oxide melts after surface relaxation were evaluated. Soft X-ray absorption spectroscopy of glass powders after heat treatment to promote surface relaxation, and the use of a PIM to perform classical MD simulations of a melt with vacuum/liquid interfaces, were used to identify the structural features of the ionic distribution in the surface region. The results obtained by the two methods were consistent with each other and indicated that BO ions are preferentially formed in the surface region by vertex connections of Al- or Si-containing polymorphs. The detailed conclusions are as follows.

1. In the case of the Al_2O_3–CaO system, Al^{3+} ions tetrahedrally coordinated with oxygen ions are preferentially distributed in the surface region, some of which connect to provide BO ions. With increasing Al_2O_3 content to 50 mol%, the preference for AlO_4 coordination becomes significant.
2. In the case of the Al_2O_3–CaO–SiO_2 system, the addition of a small amount of SiO_2 considerably changes the ionic coordination states in the surface region; Si cations are not segregated at the surface. Although Si cations are a minor component, they form various coordination states with oxygen ions, for example, SiO_4 and SiO_6. The addition of SiO_2 causes the proportion of AlO_4 to decline, while those of AlO_5 and AlO_6 are enhanced, in the bulk. However, in the surface region, SiO_4 and AlO_4 units tend to be segregated. They partially combine with each other at their vertexes to form BO ions coordinated with either Al or Si cations. The preferential distribution of these BO ions therefore contributes to the surface relaxation of the oxide melt.

AUTHOR CONTRIBUTIONS

The corresponding author, Assoc. Prof. Masanori Suzuki proposed a research strategy, performed the experimental work of XANES spectroscopy and the MD simulation, and prepared the manuscript. Mr. Yusuke Asano contributed to both the XANES spectroscopy and the simulation studies. Assoc. Prof. Yoshiki Ishii assisted in the simulation study, particularly in the analysis of ionic distribution.

ACKNOWLEDGMENTS

This work was financially supported by the Japan Society for the Promotion of Science KAKENHI (Grants-in-Aid for Scientific Research) Number JP21H01683. The results of soft X-ray absorption analyses were obtained by the subject numbers S19010, S20003, and S22016 supported by the Ritsumeikan University SR Center (Shiga, Japan). We thank Dr. Toyonari Yaji (Ritsumeikan University SR Center, Japan) and Dr. Daisuke Shibata (Ritsumeikan University SR Center, Japan) for assistance with the X-ray absorption measurements. Molecular dynamics simulations were performed at the Research Center for Computational Science, Okazaki, Japan, by the subject numbers 21-IMS-C097, 22-IMS-C097, and 23-IMS-C084. We thank Dr. Norimasa Umesaki (previously at Osaka University, Japan) for suggestions on both X-ray absorption analysis and molecular dynamics simulations. Finally, we warmly thank Mr. Yuya Yonetani (graduate student at Osaka University, Japan) for his preliminary experimental work.

ORCID

Masanori Suzuki https://orcid.org/0000-0003-1601-2842

Yoshiki Ishii https://orcid.org/0000-0003-0102-9326

REFERENCES

1. Mukai K. Marangoni flows and corrosion of refractory walls. Phil Trans R Soc Lond Ser A. 1998;356(1739):1015–26.
2. Fagerlund K, Sun S, Jahanshahi S. Effect of Marangoni-induced flow on the rate of refractory dissolution in molten slags. Scand J Metall. 2002;31(6):359–66.
3. Luz AP, Tomba Martinez AG, López F, Bonadia P, Pandolfelli VC. Slag foaming practice in the steelmaking process. Ceram Int. 2018;44(8):8727–41.
4. Kojima K, Suzuki M, Tanaka T. Distribution and reduction in P concentration of submerged arc welding slag – trials for reusing welding slag as welding flux. Quart J Jpn Weld Soc. 2018;36(3):167–74.
5. Zheng D, Ma G, Zhang X, Liu M, Xu J. Effect of CaO/Al_2O_3 on structure, viscosity, and surface tension of electroslag remelting-type CeO_2-bearing slag. J Iron Steel Res Int. 2023;30:717–25.
6. Yuan H, Dan Z, Wang Q, He S. Contact angle and adhesion of $CaO\text{-}SiO_2$- and $CaO\text{-}Al_2O_3$-based mold slags on solid steel of various compositions. J Mater Res Technol. 2020;9(4):7828–37.
7. Han SM, Park JG, Sohn I. Surface kinetics of nitrogen dissolution and its correlation to the slag structure in the $CaO\text{-}SiO_2$, $CaO\text{-}Al_2O_3$, and $CaO\text{-}SiO_2\text{-}Al_2O_3$ slag system. J Non-cryst Solids. 2011;357:2868–75.
8. Lei J, Yang W, Sheng GY, Wu T, Wang HC. Effects of BaO content and CaO/Al_2O_3 ratio on the properties and structure of aluminate slag. Metall Mater Trans B. 2022;53(4):2239–47.
9. Tanaka T, Hack K, Iida T, Hara S. Application of thermodynamic databases to the evaluation of surface tensions of molten alloys, salt mixtures and oxide mixtures. Z Metallkd. 1996;87(5):380–89.
10. King TB. The surface tension and structure of silicate slags. J Soc Glass Technol. 1951;35:241–59.
11. Tanaka T, Hara S, Ogawa M, Ueda T. Thermodynamic evaluation of the surface tension of molten salt mixtures in common ion alkali–halide systems. Z Metallkd. 1998;89(5):368–74.
12. Tanaka T, Hara S. Thermodynamics of surface tension of molten salt mixtures. Electrochemistry. 1999;67(6):573–79.
13. Livey DT, Murray P. Surface energies of solid oxides and carbides. J Am Ceram Soc. 1956;39(11):363–72.
14. Tanaka T, Kitamura T, Back IA. Evaluation of surface tension of molten ionic mixtures. ISIJ Int. 2006;46(3):400–406.
15. Nakamoto M, Kiyose A, Tanaka T, Holappa L, Hämäläinen M. Evaluation of the surface tension of ternary silicate melts containing Al_2O_3, CaO, FeO, MgO or MnO. ISIJ Int. 2007;47(1):38–43.
16. Nakamoto M, Tanaka T, Holappa L, Hämäläinen M. Surface tension evaluation of molten silicates containing surface-active components (B_2O_3, CaF_2 or Na_2O). ISIJ Int. 2007;47(2):211–16.
17. Krinochkin EV, Kurochkin KT, Umrikhin PV. Physical chemistry of surface phenomena in melts. 1971.
18. Kim AS, Akberdin AA, Kulikov IS. Viniti (USSR). 1981.
19. Elyutin VP, Mitin BS, Anisimov YS. Surface tension and density of aluminamagnesia and alumina-calcia melts. Izv VUZov Chern Met. 1974;42(4).
20. Wegener M, Muhmood L, Sun S, Deev AV. Surface tension measurements of calcia-alumina slags: a comparison of dynamic methods. Metall Mater Trans B. 2015;46:316–27.
21. Nakajima K. Estimation of surface tension for multicomponent silicate melts. J Iron Steel Inst Jpn. 1994;80(8):599–604.
22. Paras J, Takeda O, Wu M, Allanore A. The surface tension and density of molten Sc_2O_3, La_2O_3, Y_2O_3, Al_2O_3, and MgO measured via a pendant droplet method. Metall Mater Trans B. 2022;53:2077–87.
23. Xu J, Zhang J, Chen D, Sheng M, Weng W. Effects of MgO content and CaO/Al_2O_3 ratio on surface tension of calcium aluminate refining slag. J Cent South Univ. 2016;23:3079–84.
24. Mukai K, Ishikawa T. Surface tension measurements on liquid slags in $CaO\text{-}SiO_2$, $CaO\text{-}Al_2O_3$ and $CaO\text{-}Al_2O_3\text{-}SiO_2$ systems by a pendant drop method. J Japan Inst Metals. 1981;45(2):147–54.
25. Henderson G S, Groot F M F, Moulton B J A. X-ray absorption near-edge structure (XANES) spectroscopy. Rev Mineral Geochem. 2014;78:75–138.
26. Yogi C, Takamatsu D, Yamanaka K, Arai H, Uchimoto Y, Kojima K, et al. Soft X-ray absorption spectroscopic studies with different probing depths: effect of an electrolyte additive on electrode surfaces. J Power Source. 2014, 248:994–99.
27. Bilovol V, Ferrari S, Derewnicka D, Saccone FD. XANES and XPS study of electronic structure of Ti-enriched Nd–Fe–B ribbons. Mat Chem Phys. 2014;146(3):269–76.
28. Drewitt JWE, Sanloup C, Bytchkov A, Brassamin S, Hennet L. Structure of $(Fe_xCa_{1-x}O)_y(SiO_2)_{1-y}$ liquids and glasses from high-energy X-ray diffraction: Implications for the structure of natural basaltic magmas. Phys Rev B. 2013;87:224201.
29. Suzuki M, Nakano S, Serizawa H, Umesaki N. *In-situ* Phase identification of crystallized compound from $2CaO{\cdot}SiO_2$–$3CaO{\cdot}P_2O_5$ liquid. ISIJ Int. 2020, , 60(6):1127–34.
30. Baborák J, Yembele M, Vařák P, Ory S, Véron E, Pitcher MJ, et al. Key melt properties for controlled synthesis of glass beads by

aerodynamic levitation coupled to laser heating. Int J Appl Glass Sci. 2023;14(3):455–67.
31. Sakka S, Machenzie JD. Relation between apparent glass transition temperature and liquids temperature for inorganic glasses. J Non-cryst Solids. 1971;6(2):145–62.
32. Ravel B, Newville M. ATHENA, ARTEMIS, HEPHAESTUS: data analysis for X-ray absorption spectroscopy using IFEFFIT. J Synchr Radiat. 2005;12:537–41.
33. Salanne M, Simon C, Turq P, Madden PA. Simulation of the liquid-vapor interface of molten $LiBeF_3$. C R Chimie 2007;10(10-11):1131–36.
34. Ishii Y, Salanne M, Charpentier T, Shiraki K, Kasahara K, Ohtori N. A DFT-based aspherical ion model for sodium aluminosilicate glasses and melts. J Phys Chem C. 2016;120:24370–81.
35. Pacaud F, Delaye JM, Charpentier T, Cormier L, Salanne M. Structural study of Na_2O–B_2O_3–SiO_2 glasses from molecular simulations using a polarizable force field. J Chem Phys. 2017;147:161711.
36. Tesson S, Louisfrema W, Salanne M, Boutin A, Rotenberg B, Marry V. Classical polarizable force field to study dry charged clays and zeolites. J Phys Chem C. 2017;121:9833–46.
37. Salmon PS, Moody GS, Ishii Y, Pizzy KJ, Polidori A, Salanne M, et al. Pressure induced structural transformations in amorphous $MgSiO_3$ and $CaSiO_3$. J Non-cryst Solids X. 2019;3:100924.
38. Errington JR, Debenedetti PG. Relationship between structural order and the anomalies of liquid water. Nature. 2001;409:318–21.
39. Henderson GS, Neuville DR, Cormier L. An O K-edge XANES study of calcium aluminates. Canad J Chem. 2007;85:801–5.
40. Jiang N, Spence JCH. Interpretation of oxygen K pre-edge peak in complex oxides. Ultramicroscopy. 2006;106:215–19.
41. Jiang N. Structure and composition dependence of oxygen *K* edge in $CaAl_2O_4$. J Appl Phys. 2006;100:013703.
42. Kato Y, Shimizu K, Matsushita N, Yoshida T, Yoshida H, Satsuma A, et al. Quantification of aluminium coordinations in alumina and silica-alumina by Al K-edge XANES. Phys Chem Chem Phys. 2001;3:1925–29.
43. McKeown DA, Waychunas GA. Brown GE Jr. EXAFS study of the coordination environment of aluminum in a series of silica-rich glasses and selected minerals within the Na_2O-Al_2O_3-SiO_2 system. J. Non-cryst. Solids. 1985;74:349–71.
44. Cabaret D, Sainctavit P, Ildefonse P, Flank AM. Full multiple-scattering calculations on silicates and oxides at the Al K edge. J Phys Condens Matter. 1996;8:3691–704.
45. Taylor M, Brown G E Jr. Structure of mineral glasses-I. The feldspar glasses $NaAlSi_3O_8$, $KAlSi_3O_8$, $CaAl_2Si_2O_8$. Geochim Cosmochim Acta. 1978;43:61–75.
46. Allu AR, Gaddam A, Ganisetti S, Balaji S, Siegel R, Mather GC, et al. Structure and crystallization of alkaline-earth aluminosilicate glasses: prevention of the alumina-avoidance principle. J Phys Chem B. 2018;122(17):4737–47.
47. Ganisetti S, Gaddam A, Kumar R, Balaji S, Mather GC, Pascual MJ, et al. Elucidating the formation of Al-NBO bonds, Al-O-Al linkages and clusters in alkaline-earth aluminosilicate glasses based on molecular dynamics simulations. Phys Chem Phys. 2019;21(43):23966–77.
48. Li D, Bancroft GM, Fleet ME, Feng XH. Silicon K-edge XANES spectra of silicate minerals. Phys Chem Miner. 1995;22:115–22.
49. Li D, Bancroft GM, Fleet ME. Coordination of Si in Na_2O-SiO_2-P_2O_5 glasses using Si *K*- and *L*-edge XANES. Am Miner. 1996;81:111–18.
50. Butler JAV., The thermodynamics of the surfaces of solutions. Proc R Soc Lond A. 1932;135:348–75.

SUPPORTING INFORMATION

Additional supporting information can be found online in the Supporting Information section at the end of this article.

How to cite this article: Suzuki M, Asano Y, Ishii Y. Surface ionic coordination of Al_2O_3–CaO–based molten slag induced by structural relaxation. J Am Ceram Soc. 2024;1–13.
https://doi.org/10.1111/jace.19818